Performance Analysis of Network Sensing in the Distributed MIMO Radar System

Yi Song[1], Kangda Zhi[1], Tianyu Yang[1], Shuangyang Li[1], Philippe Ciblat[2] and Giuseppe Caire[1]

***Abstract*—This paper investigates the network sensing problem in a distributed multiple-input multiple-output (MIMO) radar system. We first formulate the received signal model in distributed MIMO systems as a function of the target's location. Based on the problem formulation, we derive the Cramér-Rao lower bound (CRLB) of the location estimation error for a single target, whose dependence on the layout of the transmitters (TXs) and receivers (RXs) is revealed. Using the tools from stochastic geometry, we then model the locations of TXs and RXs as homogeneous Poisson Point Process (PPP) and investigate the network-level sensing performance. Particularly, we derive the scaling law for the average estimation error, revealing the impact of various system parameters such as the number of antennas, SNR, TX/RX densities, and path loss exponent. More importantly, we unveil that the estimation error scales with the SNR and the number of antennas to the power of -1, and with the TX/RX densities to the power of $-\gamma/2$, where γ is the path loss exponent. Our numerical results confirm the accuracy of our theoretical derivations and the correctness of conclusions.**

***Index Terms*—Cramér-Rao lower bound (CRLB), Poisson Point Process (PPP), network-level sensing performance**

I. Introduction

Network sensing is becoming increasingly important for the next-generation wireless system, especially with the advent of integrated sensing and communication (ISAC) technologies. ISAC enables both communication and radar functions using the same hardware, spectrum, and signals, offering key advantages such as reduced cost, improved spectral efficiency, and enhanced power efficiency, compared to systems requiring separated transceiver designs [1–7]. These features benefit a wide range of applications, including autonomous driving for environmental sensing, smart home and building monitoring, and smart city traffic management [8].

The application of network sensing is a natural step beyond the conventional ISAC by exploiting the massively deployed base stations in cellular and cell-free wireless communications [9]. One promising application of network sensing is estimating the location of the target using wireless communication signals transmitted by transmitters (TXs). These signals, once reflected from the target and received by receivers (RXs), carry valuable information about the target's position. By analyzing the received signals, the location of the target can be inferred. A well-known method based on exploiting the bistatic ranges (BRs), i.e., the sum of TX-target and target-RX distances, was proposed in [10], where a closed-form least-square (LS) solution to a set of elliptic equations was derived to estimate the target's position. Another approach, presented in [11], involves discretizing the coverage range into grids and applying hypothesis testing (HT) in each grid to determine whether the target is present. Building upon the grid-based approach, [12] reformulated the network sensing as a compressive sensing problem by modeling the received signal response at each grid point and applied sparse Bayesian learning (SBL) to estimate the targets' locations. In addition, [13] introduced a method that directly senses the target in the beamspace by exploiting the beamspace response, whose performance can be effectively analyzed based on pairwise error probability (PEP) [14].

In light of these developments, this paper provides a general performance analysis for single-target location estimation in network sensing, using the Cramér-Rao lower bound (CRLB) as a metric. We first formulate a concise system model that reveals how the target location affects the received signals, in the presence of multiple antennas at each TX and RX. Based on this model, we extend existing CRLB derivations of [15] to include the contributions of multiple antennas, and highlight the exact dependence of the derived CRLB on the specific TX/RX locations. To gain insights into network-level sensing performance, we further model the deployment of TX and RX as practical homogeneous Poisson Point Processes (PPPs), which enables us to derive the large-scale performance on the average CRLB. This result characterizes the theoretical limits of network sensing as a function of various system parameters such as the number of antennas, signal-to-noise ratio (SNR), path loss exponent, and TX/RX densities. Unlike existing work, such as [16], which uses approximations, our derivations apply rigorous lower bounds to the CRLB, where a direct connection to the system parameters is unveiled.

II. Distributed MIMO radar system with a single target

We consider a distributed MIMO radar system with N_t TXs and N_r RXs. Each TX is equipped with M_t uniform linear array (ULA) antennas and centrally located at $\mathbf{d}_k^t = (x_k^t, y_k^t)$ for all $k \in [N_t]$ [1], while each RX is equipped with M_r ULA antennas and centrally located at $\mathbf{d}_\ell^r = (x_\ell^r, y_\ell^r)$ for all $\ell \in [N_r]$. In this paper, a *single* sensing target at location $\mathbf{d}_s = (x, y)$ is considered.

We assume that N_t TXs send signals simultaneously and denote the transmitted signal from the k-th TX as $\sqrt{\rho_s} s_k(t)$,

[1]Communications and Information Theory Group (CommIT), Technische Universität Berlin, 10587 Berlin, Germany (e-mail: {yi.song, kangda.zhi, tianyu.yang, shuangyang.li, caire}@tu-berlin.de).

[2]LTCI, Telecom Paris, Institut Polytechnique de Paris, 91120 Palaiseau, France (email: philippe.ciblat@telecom-paris.fr)

The work of Y. Song and G. Caire have been supported by DFG Gottfried Wilhelm Leibniz-Preis.

[1]The notation $[N]$ defines the set $\{1, \cdots, N\}$.

where ρ_s is the normalized SNR. Assuming that the beamforming vector for k-th TX is given as $\mathbf{w}_k \in \mathbb{C}^{M_t \times 1}$ with normalized energy, i.e., $\|\mathbf{w}_k\|^2 = 1$, the received signal for ℓ-th RX can be obtained by the reflection from the sensing target, which is given by [11]

$$\mathbf{r}_\ell(t) = \sum_{k=1}^{N_t} \alpha_{k,\ell} \mathbf{b}(\theta_\ell^r) s_k(t - \tau_{k,\ell}) + \mathbf{n}_\ell(t), \tag{1}$$

and we define $\alpha_{k,\ell}$ as

$$\alpha_{k,\ell} \triangleq \sigma \sqrt{\frac{\rho_s L_\ell^r L_k^t c^2}{(4\pi)^3 f_c^2}} \mathbf{a}^{\mathsf{H}}(\theta_k^t) \mathbf{w}_k, \tag{2}$$

where $L_\ell^r \triangleq \|\mathbf{d}_\ell^r - \mathbf{d}_s\|^{-\gamma}$ and $L_k^t \triangleq \|\mathbf{d}_k^t - \mathbf{d}_s\|^{-\gamma}$ denote the path loss in the *transmission* link between the k-th TX and the target and *reflection* link between the target and the ℓ-th RX, respectively, γ is the path-loss exponent, σ denotes the radar cross section (RCS), $\tau_{k,\ell} = \frac{\|\mathbf{d}_\ell^r - \mathbf{d}_s\| + \|\mathbf{d}_k^t - \mathbf{d}_s\|}{c}$ is the propagation delay of the transmission and reflection links with light speed c, f_c denotes the central frequency, and $\mathbf{n}_\ell(t) \in \mathbb{C}^{M_r \times 1}$ denotes the additive complex Gaussian noise, i.e., $\mathbf{n}_\ell(t) \sim \mathcal{CN}(\mathbf{0}, \mathbf{I}_{M_r})$. Moreover, θ_k^t denotes the angle-of-departure (AoD) for the k-th TX, while θ_ℓ^r denotes the angle-of-arrival (AoA) for the ℓ-th RX, and θ_k^t and θ_ℓ^r are given respectively as

$$\theta_k^t = \arctan\left(\frac{x_k^t - x}{y_k^t - y}\right), \tag{3}$$

$$\theta_\ell^r = \arctan\left(\frac{x_\ell^r - x}{y_\ell^r - y}\right). \tag{4}$$

In (1), $\mathbf{a}(\theta_k^t) \in \mathbb{C}^{M_t \times 1}$ and $\mathbf{b}(\theta_\ell^r) \in \mathbb{C}^{M_r \times 1}$ represent the array response vectors at angles θ_k^t and θ_ℓ^r for the k-th TX and ℓ-th RX, respectively, i.e.,

$$\mathbf{a}(\theta_k^t) = [1, \cdots, e^{-j\pi(M_t-1)\sin\theta_k^t}]^{\mathsf{T}}, \tag{5}$$

$$\mathbf{b}(\theta_\ell^r) = [1, \cdots, e^{-j\pi(M_r-1)\sin\theta_\ell^r}]^{\mathsf{T}}. \tag{6}$$

In this paper, we aim to discover how parameters affect the performance of estimating the location of the sensing target based on the received signals. To facilitate the analysis, the following assumptions and definitions are applied.

Definition 1: The *effective bandwidth* β_k for transmitted signal $s_k(t)$ is given by [15]

$$\beta_k^2 = \int f^2 |S_k(f)|^2 df, \quad \forall k \in [N_t], \tag{7}$$

where $S_k(f)$ is the frequency response of transmitted signal $s_k(t)$.

Assumption 1: The waveform for each TX is *energy normalized*, i.e., $\int_T |s_k(t)|^2 \mathrm{d}t = 1$, where T is the common duration of all transmitted waveforms.

Assumption 2: The transmitted signals are approximately *orthogonal* among different TXs with any time delay τ of interest[2], i.e,

$$\int_T s_k(t) s_{k'}^*(t-\tau) \mathrm{d}t \approx \begin{cases} 0 & \text{if } k \neq k', \\ 1 & \text{if } k = k', \end{cases} \tag{8}$$

[2]This assumption is reasonable in a Code-Division Multiple Access (CDMA) system, which is commonly adopted in related studies [15].

where $(\cdot)^*$ is the conjugate operator.

Assumption 3: $\alpha_{k,\ell}$ and $\tau_{k,\ell}$ in (1) are approximately *independent* [3].

A. Cramér–Rao Lower Bound

Given the received signal in (1) for all $\ell \in [N_r]$, we aim to derive the CRLB [17]. For the network sensing problem, the vector of unknown parameters is given by

$$\boldsymbol{\phi} = [x, y, \boldsymbol{\alpha}^{\mathsf{T}}]^{\mathsf{T}}, \tag{9}$$

where $\boldsymbol{\alpha}^{\mathsf{T}} \triangleq [\boldsymbol{\alpha}_{\mathrm{R}}^{\mathsf{T}}, \boldsymbol{\alpha}_{\mathrm{I}}^{\mathsf{T}}]$ with $\boldsymbol{\alpha}_{\mathrm{R}}$ and $\boldsymbol{\alpha}_{\mathrm{I}}$ denoted as the real and imaginary part of the vector $[\alpha_{1,1}, \alpha_{1,2}, \cdots, \alpha_{N_t,N_r}]^{\mathsf{T}} \in \mathbb{C}^{N_t N_r}$ respectively. The CRLB based on $\boldsymbol{\phi}$ can be better derived by first calculating the Fisher information matrix (FIM) for

$$\boldsymbol{\psi} = [\boldsymbol{\tau}^{\mathsf{T}}, \boldsymbol{\alpha}^{\mathsf{T}}]^{\mathsf{T}}, \tag{10}$$

where delays $\boldsymbol{\tau} = [\tau_{1,1}, \tau_{1,2}, \cdots, \tau_{N_t,N_r}]^{\mathsf{T}} \in \mathbb{R}^{N_t N_r}$, and $\boldsymbol{\alpha}$ is defined in (9). Based on (1), the log-likelihood function based on the parameters $\boldsymbol{\psi}$ is given by

$$\begin{aligned} &\ln p(\mathbf{r}|\boldsymbol{\psi}) = \ln p\left([\mathbf{r}_1^{\mathsf{T}}, \cdots, \mathbf{r}_{N_r}^{\mathsf{T}}]^{\mathsf{T}}|\boldsymbol{\psi}\right) \\ &\propto -\sum_{\ell=1}^{N_r} \int_T \left\| \mathbf{r}_\ell(t) - \sum_{k=1}^{N_t} \alpha_{k,\ell} \mathbf{b}(\theta_\ell^r) s_k(t - \tau_{k,\ell}) \right\|^2 \mathrm{d}t. \end{aligned} \tag{11}$$

Based on the log-likelihood function, the FIM with respect to the parameter vector $\boldsymbol{\psi}$ can be derived as summarized in the following lemma.

Lemma *1:* For the log-likelihood function in (11) for all $\ell \in [N_r]$, and under Assumption 1-3 and Definition 1, the FIM for the unknown parameters $\boldsymbol{\psi} = [\boldsymbol{\tau}^{\mathsf{T}}, \boldsymbol{\alpha}^{\mathsf{T}}]^{\mathsf{T}}$ is given by

$$\begin{aligned} \mathbf{J}(\boldsymbol{\psi}) &= \begin{bmatrix} -\mathbb{E}_{\mathbf{r}}[\frac{\partial^2 \ln p(\mathbf{r}|\boldsymbol{\psi})}{\partial \boldsymbol{\tau} \partial \boldsymbol{\tau}^{\mathsf{T}}}] & -\mathbb{E}_{\mathbf{r}}[\frac{\partial^2 \ln p(\mathbf{r}|\boldsymbol{\psi})}{\partial \boldsymbol{\tau} \partial \boldsymbol{\alpha}^{\mathsf{T}}}] \\ -\mathbb{E}_{\mathbf{r}}[\frac{\partial^2 \ln p(\mathbf{r}|\boldsymbol{\psi})}{\partial \boldsymbol{\alpha} \partial \boldsymbol{\tau}^{\mathsf{T}}}] & -\mathbb{E}_{\mathbf{r}}[\frac{\partial^2 \ln p(\mathbf{r}|\boldsymbol{\psi})}{\partial \boldsymbol{\alpha} \partial \boldsymbol{\alpha}^{\mathsf{T}}}] \end{bmatrix}, \\ &= \begin{bmatrix} \mathbf{S}_{\boldsymbol{\tau}} & \mathbf{0}_{N_t N_r, 2N_t N_r} \\ \mathbf{0}_{2N_t N_r, N_t N_r} & 2M_r \mathbf{I}_{2N_t N_r} \end{bmatrix}, \end{aligned} \tag{12}$$

where $\mathbf{S}_{\boldsymbol{\tau}}$ is defined as

$$\mathbf{S}_{\boldsymbol{\tau}} = 8\pi^2 M_r \operatorname{diag}\left(\left\{|\alpha_{k,\ell}|^2 \beta_k^2\right\}_{k \in [N_t], \ell \in [N_r]}\right). \tag{13}$$

Proof: The proof follows by extending the derivation of the CRLB from [15] to the MIMO scenario. ■

Each diagonal element of the FIM quantifies the amount of information in the received signal about a specific unknown parameter, reflecting the sensitivity of the likelihood function to variations in that parameter. Higher values indicate more sensitivity. For example, the information provided by the received signals about $\tau_{k,\ell}$ is captured by the term $8\pi^2 M_r |\alpha_{k,\ell}|^2 \beta_k^2$, which depends on factors such as the distances in the TX-target and target-RX links, the SNR, the path loss exponent, and the effective bandwidth.

Using Lemma 1, we derive the FIM with respect to $\boldsymbol{\phi}$ using chain rule derivatives, and then the CRLB for target estimation.

[3]The path loss L_k^t and L_ℓ^r in the radar channel coefficients $\alpha_{k,\ell}$ are connected via the fading exponent $-\gamma$, whose impact on the CRLB can be ignored in practice. This assumption is also considered in [15].

Lemma *2:* The FIM with respect to $\boldsymbol{\phi}$ is given by

$$\begin{aligned}\mathbf{J}(\boldsymbol{\phi}) &= \begin{bmatrix} -\mathbb{E}_{\mathbf{r}}[\frac{\partial^2 \ln p(\mathbf{r}|\boldsymbol{\psi})}{\partial \mathbf{d}_s \partial \mathbf{d}_s^{\mathsf{T}}}] & -\mathbb{E}_{\mathbf{r}}[\frac{\partial^2 \ln p(\mathbf{r}|\boldsymbol{\psi})}{\partial \mathbf{d}_s \partial \boldsymbol{\alpha}^{\mathsf{T}}}] \\ -\mathbb{E}_{\mathbf{r}}[\frac{\partial^2 \ln p(\mathbf{r}|\boldsymbol{\psi})}{\partial \boldsymbol{\alpha} \partial \mathbf{d}_s^{\mathsf{T}}}] & -\mathbb{E}_{\mathbf{r}}[\frac{\partial^2 \ln p(\mathbf{r}|\boldsymbol{\psi})}{\partial \boldsymbol{\alpha} \partial \boldsymbol{\alpha}^{\mathsf{T}}}] \end{bmatrix}, \\ &= \begin{bmatrix} \mathbf{S}_{\mathbf{d}_s} & \mathbf{0}_{2\times 2N_tN_r} \\ \mathbf{0}_{2N_tN_r\times 2} & 2M_r\mathbf{I}_{2N_tN_r} \end{bmatrix}, \end{aligned} \tag{14}$$

where $\mathbf{S}_{\mathbf{d}_s}$ is given by

$$\mathbf{S}_{\mathbf{d}_s} = \sum_{k=1}^{N_t}\sum_{\ell=1}^{N_r} 8\pi^2 M_r |\alpha_{k,\ell}|^2 \beta_k^2 \mathbf{v}_{k,\ell}\mathbf{v}_{k,\ell}^{\mathsf{T}}, \tag{15}$$

with $\mathbf{v}_{k,\ell}, \forall k \in [N_t], \ell \in [N_r]$ defined as

$$\mathbf{v}_{k,\ell} = \begin{bmatrix} \frac{\partial \tau_{k,\ell}}{\partial x} \\ \frac{\partial \tau_{k,\ell}}{\partial y} \end{bmatrix} = \frac{1}{c}\begin{bmatrix} \cos\theta_k^t + \cos\theta_\ell^r \\ \sin\theta_k^t + \sin\theta_\ell^r \end{bmatrix}. \tag{16}$$

Proof: Following the chain rule for derivatives, the FIM with respect to $\boldsymbol{\phi}$ can be derived through a projection matrix, given as

$$\mathbf{J}(\boldsymbol{\phi}) = \mathbf{P}\mathbf{J}(\boldsymbol{\psi})\mathbf{P}^{\mathsf{T}}, \tag{17}$$

where $\mathbf{P}$ is derived from the derivative of $\boldsymbol{\psi}$ with respect to $\boldsymbol{\phi}$, i.e., $\mathbf{P} = \frac{\partial \boldsymbol{\psi}^{\mathsf{T}}}{\partial \boldsymbol{\phi}}$. The rest of the proof follows straightforward algebraic manipulation. ∎

Unlike $\mathbf{J}(\boldsymbol{\psi})$, the FIM with respect to $\boldsymbol{\phi}$ is not block diagonal. The off-diagonal elements in the FIM indicate the correlation between pairs of parameters. Specifically, they measure how much information about one parameter is affected by variations of another. According to the above derivations, we summarize the derived CRLB in the following theorem.

Theorem *1:* Let $\widehat{\mathbf{d}}_s$ denote the target's estimated location. The CRLB on the estimation mean squared error (MSE) of target's location $\mathbf{d}_s$ is given by

$$\begin{aligned}\mathbb{E}\left[\|\mathbf{d}_s - \widehat{\mathbf{d}}_s\|^2\right] &\geqslant [(\mathbf{J}(\boldsymbol{\phi})^{-1})]_{2\times 2} \\ &= \mathsf{tr}\left(\mathbf{S}_{\mathbf{d}_s}^{-1}\right), \end{aligned} \tag{18}$$

where $\mathbf{J}(\boldsymbol{\phi})$ and $\mathbf{S}_{\mathbf{d}_s}$ are given in (14) and (15), respectively.

We have shown in (18) that the accuracy of the target location estimation strongly depends on many parameters. In order to quantify their impacts explicitly and shed light on network-level sensing performance, we will characterize the scaling law of CRLB with respect to TX/RX densities in the coming subsection, using the tools from stochastic geometry.

B. The Scaling Law of CRLB in Distributed MIMO Radar Systems

In this subsection, we want to eliminate the effects of the specific layout of TXs and RXs by considering the large-scale average sensing performance. For the derivation, we consider the following assumptions.

Assumption 4: TXs follow a homogeneous PPP with intensity λ_t, while RXs follow an independent PPP with intensity λ_r, i.e., $(x_k^t, y_k^t) \sim \boldsymbol{\Phi}_t(\lambda_t)$ and $(x_\ell^r, y_\ell^r) \sim \boldsymbol{\Phi}_r(\lambda_r)$ [18].

Assumption 5: The effective bandwidth is the same for all TXs, i.e., $\beta_1 = \beta_2 = \cdots = \beta$.

Assumption 6: The path loss exponent is greater than 2, i.e., $\gamma > 2$, which is common for outdoor wireless scenarios.

Based on (18), a *lower bound* on the CRLB, called the Miller-Chang type CRLB [19], is derived as

$$\begin{aligned}&\mathbb{E}_{\boldsymbol{\Phi}_t,\boldsymbol{\Phi}_r}\left[\mathbb{E}\left[\|\mathbf{d}_s - \widehat{\mathbf{d}}_s\|^2\right]\right], \\ \geqslant&\mathbb{E}_{\boldsymbol{\Phi}_t,\boldsymbol{\Phi}_r}\left[\mathbb{E}_{\boldsymbol{\theta}^t,\boldsymbol{\theta}^r|\boldsymbol{\Phi}_t,\boldsymbol{\Phi}_r}\left[\mathsf{tr}\left(\mathbf{S}_{\mathbf{d}_s}^{-1}\right)\right]\right] \qquad (19) \\ \geqslant&\mathbb{E}_{\boldsymbol{\Phi}_t,\boldsymbol{\Phi}_r}\left[\mathsf{tr}\left(\left(\mathbb{E}_{\boldsymbol{\theta}^t,\boldsymbol{\theta}^r|\boldsymbol{\Phi}_t,\boldsymbol{\Phi}_r}\left[\mathbf{S}_{\mathbf{d}_s}\right]\right)^{-1}\right)\right], \qquad (20)\end{aligned}$$

where (19) follows from the law of iterated expectation, and $\boldsymbol{\theta}_t$ and $\boldsymbol{\theta}_r$ denote the sets of AoAs and AoDs. The inequality in (20) employs the Jensen's inequality. Note that the lower bound in (20) only includes the angle information in the inverse operator, which gives a rather tight bound.

Let $\eta \triangleq \frac{8\pi^2\rho_s\sigma^2\beta^2c^2}{(4\pi)^3 f_c^2}$. With this substitution, we can reorganize (20) for further approximation as follows,

$$\begin{aligned}&\mathbb{E}_{\boldsymbol{\theta}^t,\boldsymbol{\theta}^r|\boldsymbol{\Phi}_t,\boldsymbol{\Phi}_r}\left[\mathbf{S}_{\mathbf{d}_s}\right] \\ =&\mathbb{E}_{\boldsymbol{\theta}^t,\boldsymbol{\theta}^r|\boldsymbol{\Phi}_t,\boldsymbol{\Phi}_r}\left[\sum_{k=1}^{N_t}\sum_{\ell=1}^{N_r} M_r\eta L_\ell^r L_k^t |\mathbf{a}^{\mathsf{H}}(\theta_k^t)\mathbf{w}_k|^2 \mathbf{v}_{k,\ell}\mathbf{v}_{k,\ell}^{\mathsf{T}}\right] \\ \leqslant&\sum_{k=1}^{N_t}\sum_{\ell=1}^{N_r} M_r M_t \eta L_\ell^r L_k^t \mathbb{E}_{\boldsymbol{\theta}^t,\boldsymbol{\theta}^r|\boldsymbol{\Phi}_t,\boldsymbol{\Phi}_r}\left[\mathbf{v}_{k,\ell}\mathbf{v}_{k,\ell}^{\mathsf{T}}\right] \qquad (21) \\ =&\sum_{k=1}^{N_t}\sum_{\ell=1}^{N_r} \frac{M_r M_t \eta L_\ell^r L_k^t}{c^2}\begin{bmatrix}1 & 0\\ 0 & 1\end{bmatrix}, \qquad (22)\end{aligned}$$

where the inequality (21) holds due to the complex Cauchy-Schwarz-Buniakowsky inequality, i.e., $|\mathbf{a}^{\mathsf{H}}(\theta_k^t)\mathbf{w}_k|^2 \leqslant \|\mathbf{a}^{\mathsf{H}}(\theta_k^t)\|^2\|\mathbf{w}_k\|^2 = M_t$, and (22) is derived from the rotation invariant property of the PPP distribution [18]. Specifically, $\boldsymbol{\theta}_t|\boldsymbol{\Phi}_t$ and $\boldsymbol{\theta}_r|\boldsymbol{\Phi}_r$ are uniformly distributed between $-\frac{\pi}{2}$ and $\frac{\pi}{2}$, and it follows that $\mathbb{E}_{\theta|\boldsymbol{\Phi}}[\cos\theta\sin\theta] = \mathbb{E}_{\theta|\boldsymbol{\Phi}}[\cos\theta] = \mathbb{E}_{\theta|\boldsymbol{\Phi}}[\sin\theta] = 0$, and $\mathbb{E}_{\theta|\boldsymbol{\Phi}}[\cos^2(\theta)] = \mathbb{E}_{\theta|\boldsymbol{\Phi}}[\sin^2(\theta)] = 1/2$.

Remark *1:* The derivation based on (21) provides the optimal scaling law with respect to the number of transmit antennas M_t. This result can be achieved by probing all energy towards the target, thereby realizing the full beamforming gain. Although this is not practically achievable, we argue that this is a necessary simipification for deriving the lower bounds. In fact, such assumption does not change the scaling law of the system parameters of interest that will be discussed in the following.

Combing (20) with (22), a lower bound on the expected estimation error (20) using full beamforming gain can be further developed as

$$\begin{aligned}&\mathbb{E}_{\boldsymbol{\Phi}_t,\boldsymbol{\Phi}_r}\left[\mathsf{tr}\left(\left(\mathbb{E}_{\boldsymbol{\theta}^t,\boldsymbol{\theta}^r|\boldsymbol{\Phi}_t,\boldsymbol{\Phi}_r}\left[\mathbf{S}_{\mathbf{d}_s}\right]\right)^{-1}\right)\right] \\ \geqslant&\mathbb{E}_{\boldsymbol{\Phi}_t,\boldsymbol{\Phi}_r}\left[\mathsf{tr}\left(\left(\sum_{k=1}^{N_t}\sum_{\ell=1}^{N_r}\frac{M_r M_t \eta}{c^2} L_\ell^r L_k^t \mathbf{I}_2\right)^{-1}\right)\right] \\ =&2\mathbb{E}_{\boldsymbol{\Phi}_t,\boldsymbol{\Phi}_r}\left[\left(\frac{M_r M_t \eta}{c^2}\left(\sum_{\ell=1}^{N_r} L_\ell^r\right)\left(\sum_{k=1}^{N_t} L_k^t\right)\right)^{-1}\right]\end{aligned}$$

$$=\frac{2c^2}{M_rM_t\eta}\mathbb{E}_{\mathbf{\Phi}_r}\left[\left(\sum_{\ell=1}^{N_r}L_\ell^r\right)^{-1}\right]\mathbb{E}_{\mathbf{\Phi}_t}\left[\left(\sum_{k=1}^{N_t}L_k^t\right)^{-1}\right]. \quad (23)$$

Lemma *3:* Using the tools from stochastic geometry, $\mathbb{E}_{\mathbf{\Phi}_r}\left[\left(\sum_{\ell=1}^{N_r}L_\ell^r\right)^{-1}\right]$ and $\mathbb{E}_{\mathbf{\Phi}_t}\left[\left(\sum_{k=1}^{N_t}L_k^t\right)^{-1}\right]$ are given by

$$\mathbb{E}_{\mathbf{\Phi}_t}\left[\left(\sum_{k=1}^{N_t}L_k^t\right)^{-1}\right]=\Gamma\Big(1+\frac{\gamma}{2}\Big)\Big(\pi\lambda_t\Gamma\left(1-\frac{2}{\gamma}\right)\Big)^{-\frac{\gamma}{2}}, \quad (24)$$

$$\mathbb{E}_{\mathbf{\Phi}_r}\left[\left(\sum_{\ell=1}^{N_r}L_\ell^r\right)^{-1}\right]=\Gamma\Big(1+\frac{\gamma}{2}\Big)\Big(\pi\lambda_r\Gamma\left(1-\frac{2}{\gamma}\right)\Big)^{-\frac{\gamma}{2}}, \quad (25)$$

where $\Gamma(\cdot)$ is the gamma function, and also notice that $\gamma>2$.

Proof: See Appendix A. ∎

Combing (23), (24) and (25), we have the lower bound to the average target location estimation error summarized in the following theorem.

Theorem *2:* Under Assumption 1-6 and Definition 1, the scaling law of the average target location estimation error is characterized by

$$\mathbb{E}^{\text{mimo}}_{\mathbf{\Phi}_t,\mathbf{\Phi}_r}\left[\mathbb{E}\left[\|\mathbf{d}_s-\widehat{\mathbf{d}}_s\|^2\right]\right]$$
$$\geqslant\frac{2c^2}{M_rM_t\eta}\Gamma^2\Big(1+\frac{\gamma}{2}\Big)\Big(\pi\sqrt{\lambda_r\lambda_t}\Gamma\left(1-\frac{2}{\gamma}\right)\Big)^{-\gamma},\gamma>2. \quad (26)$$

Theorem 2 establishes the scaling law for the average error in estimating the position of a target, taking into account the effects of various parameters. Here are the key observations of the theorem:

- **System parameters**: The constant η, which encapsulates parameters such as effective bandwidth, carrier frequency, transmit power, and noise power, acts as a scaling factor. This factor shows how certain system-level characteristics, such as higher transmit power (ρ_s) or increased effective bandwidth (β), contribute to lowering the error bound by providing better signal clarity and information acquisition.
- **Number of antennas**: The average estimation error scales inversely with the number of TX and RX antennas, M_t and M_r. Increasing the number of antennas effectively increases spatial diversity, which allows more robust signal measurement and results in a lower CRLB.
- **Intensity for TX/RX distributions**: The TX/RX densities (λ_t and λ_r) also have significant effects on the estimation accuracy. Higher densities of TXs and RXs in a given area provides a richer spatial sampling, resulting in more measurements and thus a reduction in the CRLB. This effect is represented by the term $\left(\sqrt{\lambda_r\lambda_t}\right)^{-\gamma}$, where increasing the density reduces the error by a factor of $-\frac{\gamma}{2}$.
- **Path loss exponent**: The path loss exponent γ (typically between 2 and 4, depending on the environment) strongly influences the estimation accuracy. In particular, for $\gamma>2$, higher values of γ lead to a faster decay of the received signal power with distance, which strengthens the importance of high TX/RX intensity. The error bound is influenced by γ through terms $\Gamma^2\left(1+\frac{\gamma}{2}\right)$ and $\left(\Gamma\left(1-\frac{2}{\gamma}\right)\right)^{-\gamma}$, highlighting a nonlinear relationship between γ and estimation error.

C. Distributed Level vs. Number of Antennas per TX/RX

To provide theoretical guidelines for system design, here, we consider the *single-antenna* distributed radar system, where TXs follow PPP distribution with density $\widetilde{\lambda}_t$ and RXs also follow an independent PPP distribution with density $\widetilde{\lambda}_r$. Hence, the received signal for ℓ-th RX is given by

$$r_\ell(t)=\sum_{k=1}^{\widetilde{N}_t}\sigma\sqrt{\frac{\rho_sL_\ell^rL_k^tc^2}{(4\pi)^3f_c^2}}s_k(t-\tau_{k,\ell})+n_\ell(t),\forall\ell\in[\widetilde{N}_r]. \quad (27)$$

Following the similar steps derived in Section II-B, the estimation error of the target location in the distributed single-antenna system is thus lower bounded by

$$\mathbb{E}^{\text{single}}_{\mathbf{\Phi}_t,\mathbf{\Phi}_r}\left[\mathbb{E}\left[\|\mathbf{d}_s-\widehat{\mathbf{d}}_s\|^2\right]\right]$$
$$\geqslant\frac{2c^2}{\eta}\Gamma^2\left(1+\frac{\gamma}{2}\right)\left(\pi\sqrt{\widetilde{\lambda}_r\widetilde{\lambda}_t}\Gamma\left(1-\frac{2}{\gamma}\right)\right)^{-\gamma},\gamma>2. \quad (28)$$

To make a fair comparison between sensing performances of distributed MIMO radar systems in (26) and single-antenna radar systems in (28), we consider the following setup

$$\widetilde{\lambda}_r=M_r\lambda_r,\ \widetilde{\lambda}_t=M_t\lambda_t, \quad (29)$$

so that the two systems have, on average, the same total number of antennas. Then, when $\gamma>2$, the comparison yields the following inequality:

$$\frac{\left(\sqrt{\lambda_t\lambda_r}\right)^{-\gamma}}{M_tM_r}>\left(\sqrt{\widetilde{\lambda}_t\widetilde{\lambda}_r}\right)^{-\gamma}, \quad (30)$$

which indicates that when $\gamma>2$, **the estimation error of the target location decreases faster in the distributed single-antenna radar system than in the distributed MIMO radar system, under roughly the same number of antennas in the network**. This is because the estimation error in the single-antenna system is scaled with the density of TXs and RXs to the power of $-\frac{\gamma}{2}$ ($\gamma>2$), while in the distributed MIMO system it is scaled with the number of transmit and receive antennas to the power of -1.

III. Simulation Results

In this section, we present numerical results to evaluate the impact of different parameters on target location estimation in the single-target scenario. For the simulations, we use a system with $M_t=M_r=4$ TX/RX antenna, a bandwidth of 2 GHz, a carrier frequency of 30 GHz, and a noise power spectral density of $N_0=5\times10^{-22}$ W/Hz. The effective bandwidth is $\beta_k=0.577$ GHz, with a radar cross section (RCS) of $\sigma=1\,\text{m}^2$ and a path loss exponent of $\gamma=2.5$. We also assume a PPP intensity for the TX/RX of $\lambda_t=\lambda_r=1/30^2\,\text{m}^{-2}$. The target is positioned at $\mathbf{d}_s=(0,0)$.

To validate the effectiveness of the derived scaling law for the averaged CRLB, as given in the right-hand side of (26), we compare it with numerical results from Monte Carlo (MC) simulations using expression (18). We also perform numerical

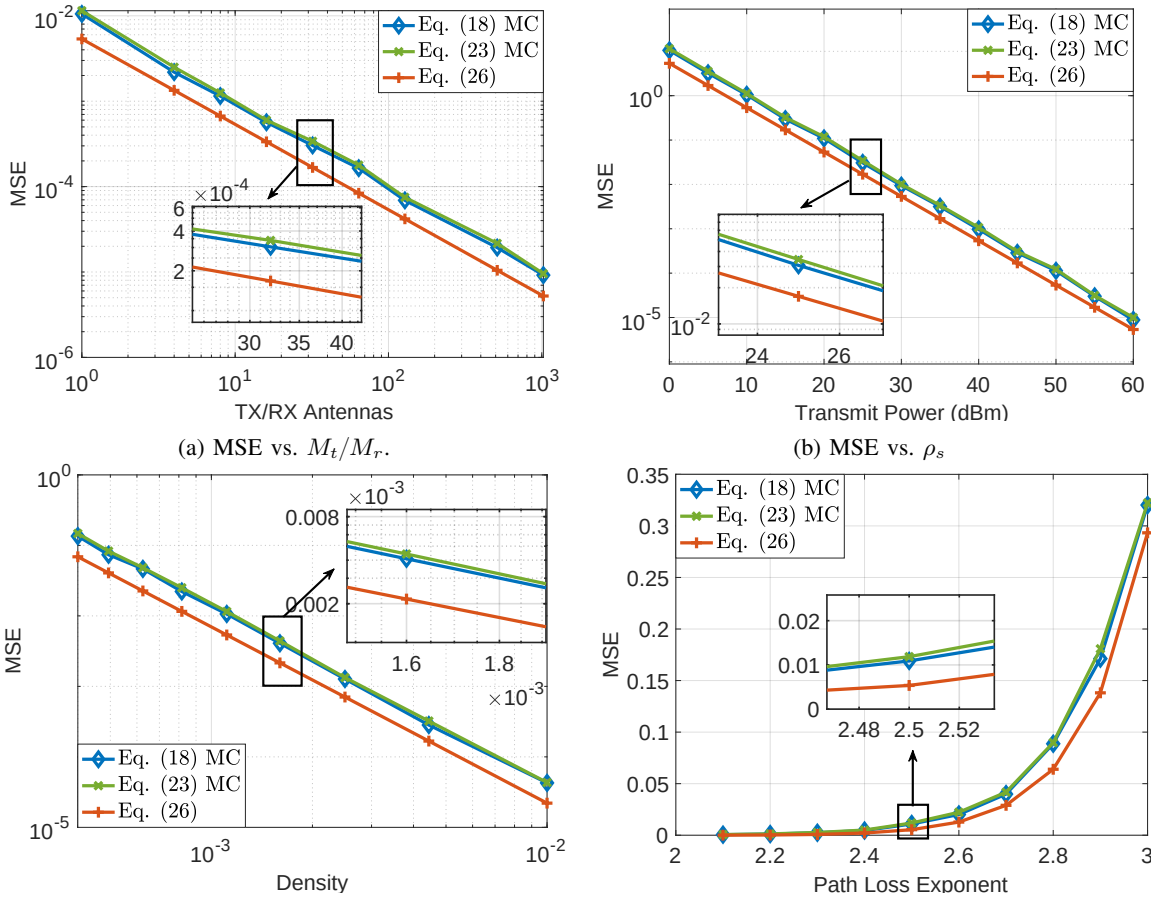

(a) MSE vs. M_t/M_r.

(b) MSE vs. ρ_s

(c) MSE vs. λ_t/λ_r.

(d) MSE vs. γ.

Fig. 1: The evaluation on various parameters.

results from MC simulations with respect to intermediate expression (23), to verify the correctness of our derivation in Lemma 3 based on the PPP properties.

In the simulations, we examine the impact of various parameters including:

- the number of TX/RX antennas in Fig. 1a,
- the SNR in Fig. 1b,
- the density of the TX/RX distribution in Fig. 1c,
- the path loss exponent in Fig. 1d.

As expected, Figure 1 shows that the theoretical result (red curve) is consistently below the other two curves, reflecting that the MC simulation based on (18) serves as an upper bound for the result in (26) due to Jensen's inequality in (20). According to theorem 2, the estimation error scales inversely with both the number of TX/RX antennas and the transmit power ρ_s, corresponding to the slopes of the red curves in Fig. 1a and Fig. 1b, respectively. Furthermore, the error scales with the intensity λ_t/λ_r to the power of $-\gamma/2$, which defines the slope of the red curve in Fig. 1c. As shown in Fig. 1, we observe that all the curves exhibit nearly identical behavior, confirming the effectiveness of the derived scaling law in Theorem 2. A small gap between the MC simulations and the closed-form expressions is observed due to the limited area of PPP in the simulation, which can be tightened by expanding the TX/RX distribution area in the simulation. The consistency between theoretical derivation and MC simulation demonstrates the value of our result for practical network-level sensing evaluation.

IV. Conclusion

In this work, we focused on the network sensing problem in the distributed MIMO radar system with simultaneous signal transmission. First, we derived the CRLB for the estimation error in the single-target scenario. Additionally, assuming that the TXs/RXs follow an independent PPP distribution, we established the scaling law for the estimation error with respect to the number of TX/RX antennas, SNR, intensity of TX/RX distribution, and path loss exponent. Numerical simulations are consistent with the theoretical analysis, confirming the accuracy of our derivations.

Appendix A
Proof of Lemma

For simplicity, we denote the function $L(\mathbf{x})$ as $\|\mathbf{x}-\mathbf{d}_s\|^{-\gamma}$, $\forall \mathbf{x} \in \mathbb{R}^2$. Based on the properties of the PPP, $\mathbb{E}_{\mathbf{\Phi}_r}\left[\left(\sum_{\ell=1}^{N_r} L_\ell^r\right)^{-1}\right]$ can be rewritten as

$$\mathbb{E}_{\mathbf{\Phi}_r}\left[\left(\sum_{\ell=1}^{N_r} L_\ell^r\right)^{-1}\right] = \mathbb{E}_{\mathbf{\Phi}_r}\left[\left(\sum_{\mathbf{x}\in\mathbf{\Phi}_r} L(\mathbf{x})\right)^{-1}\right]$$

$$=\mathbb{E}_{\mathbf{\Phi}_r}\left[\left(\int_0^\infty e^{-s\sum_{\mathbf{x}\in\mathbf{\Phi}_r}L(\mathbf{x})}ds\right)\right] \tag{31}$$

$$=\int_0^\infty \mathbb{E}_{\mathbf{\Phi}_r}\left[e^{-s\sum_{\mathbf{x}\in\mathbf{\Phi}_r}L(\mathbf{x})}\right]ds$$

$$=\int_0^\infty \mathbb{E}_{\mathbf{\Phi}_r}\left[\prod_{\mathbf{x}\in\mathbf{\Phi}_r}e^{-sL(\mathbf{x})}\right]ds$$

$$=\int_0^\infty \exp\left(-\lambda_r\int_{\mathbb{R}^2}(1-e^{-sL(\mathbf{x})})d\mathbf{x}\right)ds \tag{32}$$

$$=\int_0^\infty \exp\left(-\lambda_r\int_{\mathbb{R}^2}(1-e^{-s\|\mathbf{x}-\mathbf{d}_s\|^{-\gamma}})d\mathbf{x}\right)ds$$

$$=\int_0^\infty \exp\left(-\lambda_r\int_{\mathbb{R}^2}(1-e^{-s\|\mathbf{x}\|^{-\gamma}})d\mathbf{x}\right)ds, \tag{33}$$

where (31) holds due to the Laplace transform, and (32) holds due to the probability generating functional (PGFL) of the PPP, which states that $\mathbb{E}[\prod_{\mathbf{x}\in\mathbf{\Phi}}g(\mathbf{x})] = \exp\left(-\lambda\int_{\mathbb{R}^2}(1-g(\mathbf{x}))d\mathbf{x}\right)$ for some function $0\leqslant g(\mathbf{x})\leqslant 1$. Thus, PGFL can be used in (32) since its exponential function meets the constraint of $0\leqslant g(\mathbf{x})\leqslant 1$. (33) holds due to its shift invariance. When we transform (33) into the polar coordinates, (33) becomes

$$\int_0^\infty \exp\left(-\lambda_r\int_{\mathbb{R}^2}\left(1-e^{-s\|\mathbf{x}\|^{-\gamma}}\right)d\mathbf{x}\right)ds$$
$$=\int_0^\infty \exp\left(-2\pi\lambda_r\int_0^\infty r\left(1-e^{-sr^{-\gamma}}\right)dr\right)ds, \tag{34}$$

where according to [20, eq. (16)], we have that if $\gamma>2$, then

$$\int_0^\infty r\left(1-e^{-sr^{-\gamma}}\right)dr=\frac{1}{2}s^{\frac{2}{\gamma}}\Gamma\left(1-\frac{2}{\gamma}\right), \tag{35}$$

where $\Gamma(\cdot)$ is the Gamma function. Therefore, (33) can be rewritten as

$$\mathbb{E}_{\mathbf{\Phi}_r}\left[\left(\sum_{\ell=1}^{N_r}L_\ell^r\right)^{-1}\right]=\int_0^\infty \exp\left(-\pi\lambda_r s^{\frac{2}{\gamma}}\Gamma\left(1-\frac{2}{\gamma}\right)\right)ds$$
$$=\frac{\Gamma(\frac{\gamma}{2})}{\frac{2}{\gamma}\left(\pi\lambda_r\Gamma\left(1-\frac{2}{\gamma}\right)\right)^{\frac{\gamma}{2}}} \tag{36}$$

$$=\Gamma\left(1+\frac{\gamma}{2}\right)\left(\pi\lambda_r\Gamma\left(1-\frac{2}{\gamma}\right)\right)^{-\frac{\gamma}{2}},\quad \gamma>2, \tag{37}$$

where (36) holds due to the integral of $\frac{e^{-\beta x^n}}{x^m}$ in [21, P.109] and the fact that $\Gamma(1+t)=t\Gamma(t)$ results in (37). In the same way, $\mathbb{E}_{\mathbf{\Phi}_t}\left[\left(\sum_{k=1}^{N_t}L_k^t\right)^{-1}\right]$ can be simplified as (24).

REFERENCES

[1] T. Wild, V. Braun, and H. Viswanathan, "Joint design of communication and sensing for beyond 5g and 6g systems," *IEEE Access*, vol. 9, pp. 30 845–30 857, 2021.

[2] F. Liu, Y. Cui, C. Masouros, J. Xu, T. X. Han, Y. C. Eldar, and S. Buzzi, "Integrated sensing and communications: Towards dual-functional wireless networks for 6G and beyond," *IEEE J. Sel. Area Commun.*, Mar. 2022.

[3] M. Kobayashi, G. Caire, and G. Kramer, "Joint state sensing and communication: Optimal tradeoff for a memoryless case," in *Proc. IEEE Int. Symp. Inf. Theory (ISIT)*, Jun. 2018, pp. 111–115.

[4] M. Kobayashi, H. Hamad, G. Kramer, and G. Caire, "Joint state sensing and communication over memoryless multiple access channels," in *Proc. IEEE Int. Symp. Inf. Theory (ISIT)*, Jul. 2019, pp. 270–274.

[5] M. Ahmadipour, M. Kobayashi, M. Wigger, and G. Caire, "An information-theoretic approach to joint sensing and communication," *IEEE Trans. Inf. Theory, early access*, May 2022.

[6] S. Li and G. Caire, "On the capacity and state estimation error of "beam-pointing" channels: The binary case," *IEEE Trans. Inf. Theory*, vol. 69, no. 9, p. 5752–5770, Sep. 2023.

[7] S. Li, W. Yuan, C. Liu, Z. Wei, J. Yuan, B. Bai, and D. W. K. Ng, "A novel ISAC transmission framework based on spatially-spread orthogonal time frequency space modulation," *IEEE J. Sel. Areas Commun.*, vol. 40, no. 6, pp. 1854–1872, Jun. 2022.

[8] Y. Cui, F. Liu, X. Jing, and J. Mu, "Integrating sensing and communications for ubiquitous iot: Applications, trends, and challenges," *IEEE Network*, vol. 35, no. 5, pp. 158–167, 2021.

[9] K. Meng, C. Masouros, A. P. Petropulu, and L. Hanzo, "Cooperative isac networks: Opportunities and challenges," *IEEE Wireless Commun.*, pp. 1–8, 2024.

[10] M. Dianat, M. R. Taban, J. Dianat, and V. Sedighi, "Target localization using least squares estimation for MIMO radars with widely separated antennas," *IEEE Trans. Aerosp. Electron. Syst.*, vol. 49, no. 4, pp. 2730–2741, 2013.

[11] S. K. Dehkordi, L. Pucci, P. Jung, A. Giorgetti, E. Paolini, and G. Caire, "Multistatic parameter estimation in the near/far field for integrated sensing and communication," *IEEE Trans. Wireless Commun.*, pp. 1–1, 2024.

[12] T. Yang, S. Li, Y. Song, K. Zhi, and G. Caire, "Cooperative multistatic target detection in cell-free communication networks," *arXiv preprint arXiv:2410.16140*, 2024.

[13] Y. Song, F. Pedraza, S. Li, S. Li, H. Yu, and G. Caire, "Compressed sensing inspired user acquisition for downlink integrated sensing and communication transmissions," in *Proc. IEEE Int. Conf. Commun. (ICC)*, 2024, pp. 5293–5298.

[14] S. Li, J. Yuan, W. Yuan, Z. Wei, B. Bai, and D. W. K. Ng, "Performance analysis of coded OTFS systems over high-mobility channels," *IEEE Trans. Wireless Commun.*, vol. 20, no. 9, pp. 6033–6048, Sep. 2021.

[15] H. Godrich, A. M. Haimovich, and R. S. Blum, "Target localization accuracy gain in MIMO radar-based systems," *IEEE Trans. Inf. Theory*, vol. 56, no. 6, pp. 2783–2803, 2010.

[16] K. Meng, C. Masouros, A. P. Petropulu, and L. Hanzo, "Cooperative ISAC networks: Performance analysis, scaling laws and optimization," 2024.

[17] S. M. Kay, "Statistical signal processing: estimation theory," *Prentice Hall*, vol. 1, pp. Chapter–3, 1993.

[18] S. N. Chiu, D. Stoyan, W. S. Kendall, and J. Mecke, *Stochastic geometry and its applications*. John Wiley & Sons, 2013.

[19] G. Tavares, L. Tavares, and M. Piedade, "On the Miller-Chang lower bound for NDA carrier phase estimation," *IEEE Trans. Commun.*, vol. 52, no. 11, pp. 1867–1871, Nov. 2004.

[20] Y. Xiong, S. Han, and Q. Wu, "Performance limits of passive localization with randomly distributed transmitters and receivers," in *Proc. 8th IEEE Int. Conf. Wireless Commun. Signal Process. (WCSP)*, 2016, pp. 1–5.

[21] I. S. Gradshteyn and I. M. Ryzhik, *Table of integrals, series, and products*. Academic press, 2014.